GEOFLUIDS
Geofluids (2015) 15, 321–337 doi: 10.1111/gfl.12097

Development of connected permeability in massive crystalline rocks through hydraulic fracture propagation and shearing accompanying fluid injection

G. PREISIG[1], E. EBERHARDT[1], V. GISCHIG[1], V. ROCHE[2], M. VAN DER BAAN[2], B. VALLEY[3], P. K. KAISER[4], D. DUFF[4] AND R. LOWTHER[5]

[1]Geological Engineering, EOAS, The University of British Columbia, Vancouver, BC, Canada; [2]Department of Physics, University of Alberta, Edmonton, AB, Canada; [3]Geological Institute, ETH Zurich, Zurich, Switzerland; [4]CEMI - Centre for Excellence in Mining Innovation, Sudbury, ON, Canada; [5]Newcrest Mining Limited, Cadia Valley Operations, South Orange, NSW, Australia

ABSTRACT

The ability to generate deep flow in massive crystalline rocks is governed by the interconnectivity of the fracture network and its permeability, which in turn is largely dependent on the *in situ* stress field. The increase of stress with depth reduces fracture aperture, leading to a decrease in rock mass permeability. The frequency of natural fractures also decreases with depth, resulting in less connectivity. The permeability of crystalline rocks is typically reduced to about 10^{-17}–10^{-15} m^2 at targeted depths for enhanced geothermal systems (EGS) applications, that is, >3 km. Therefore, fluid injection methods are required to hydraulically fracture the rock and increase its permeability. In the mining sector, fluid injection methods are being investigated to increase rock fragmentation and mitigate high-stress hazards due to operations moving to unprecedented depths. Here as well, detailed understanding of permeability and its enhancement is required. This paper reports findings from a series of hydromechanically coupled distinct-element models developed in support of a hydraulic fracture experiment testing hypotheses related to enhanced permeability, increased fragmentation, and modified stress fields. Two principal injection designs are tested as follows: injection of a high flow rate through a narrow-packed interval and injection of a low flow rate across a wider packed interval. Results show that the development of connected permeability is almost exclusively orthogonal to the minimum principal stress, leading to strongly anisotropic flow. This is because of the stress transfer associated with opening of tensile fractures, which increases the confining stress acting across neighboring natural fractures. This limits the hydraulic response of fractures and the capacity to create symmetric isotropic permeability relative to the injection wellbore. These findings suggest that the development of permeability at depth can be improved by targeting a set of fluid injections through smaller packed intervals instead of a single longer injection in open boreholes.

Key words: fracture network, hard rocks, hydraulic fracturing, numerical modeling, permeability, reservoir enhancement, shearing, stress transfer

Received 13 January 2014; accepted 1 August 2014

Corresponding author: Giona Preisig, Geological Engineering, EOAS, The University of British Columbia, 2207 Main Mall, V6T 1Z4 Vancouver, BC Canada.
Email: gpreisig@eos.ubc.ca. Tel: +1-604-827-1502. Fax: +1-604-822-6088.

Geofluids (2015) **15**, 321–337

INTRODUCTION

Rock mass permeability is the foremost hydromechanical parameter for industries concerned with geofluids extraction, including groundwater, geothermal water, oil, and gas. In massive crystalline rocks, often favored for enhanced geothermal system (EGS) projects, permeability is governed by fracture connectivity and aperture. However, the dependency of fracture permeability on mechanical stresses limits the accessibility of geofluids located in reservoirs at substantial depths. The increase of stress with depth leads to the closure of fracture aperture, which results in the following: (i) reduced permeability, (ii) decreased fracture network connectivity, and (iii) increased

rock stiffness (Louis 1969; Tsang & Witherspoon 1981; Durham 1997; Rutqvist & Stephansson 1996; Ingebritsen & Manning 2010; Preisig *et al.* 2012). There are exceptions related to the presence of highly conductive fractures; however, such structures are sparse.

In this context, injection of pressurized fluid for hydraulic treatments is critical for enhancing the interconnectivity of fracture permeability in tight rock masses. This form of preconditioning, that is, altering the rock mass properties for engineering purposes, is widely used in the development of deep geothermal power production and shale gas extraction, where focus is placed on enhancing the rock mass permeability. Likewise, hydraulic fracturing is being utilized in the mineral industry to ensure suitable fragmentation in block caving operations (Fairhurst 2013; Jung 2013; Kaiser *et al.* 2013), as well as being investigated as a means to mitigate high-stress hazards, for example, rock bursting, in deep mining operations.

Two injection procedures may be employed in this context: hydraulic fracturing (HF) and hydraulic shearing (HS). The main difference is that HF aims to initiate and propagate new tensile fractures through injection, whereas HS tries to shear pre-existing natural discontinuities. It should be noted that HF and HS are conceptual end members and will often act to varying degrees in combination. To initiate a new hydraulic fracture, the injection pressure must exceed the so-called breakdown pressure which is driven by the stress concentration around the borehole wall and the tensile strength of the rock. The magnitude of the breakdown pressure will depend on the stress ratio and will typically be larger than minimum principal stress σ_3. The injection pressure to propagate a hydraulic fracture or to propagate in tension a pre-existing natural fracture in which borehole pressure may have infiltrated is typically less than the breakdown pressure but still has to exceed σ_3. Consequently, it is conservative to state that the minimum fluid injection pressure p_f required to perform HF is as follows:

$$p_f > \sigma_3 \tag{1}$$

It is also expected that the hydraulic fracture will close when the pressure in the opened fracture dissipates, resulting in a small net permeability increase. In the case of hydraulic shearing (HS), the objective is to induce slip, which assuming zero cohesion along a rough tensile fracture surface can be expressed using the Mohr–Coulomb shear failure criterion

$$|\tau| \geq \mu\,(\sigma_n - p_f) \tag{2}$$

where τ is the shear stress, μ is the coefficient of friction of the fracture, that is, $\mu = \tan(\phi)$, and σ_n is the stress acting normal to the fracture plane. The fluid injection pressure p_f required to mobilize shear slip along the fracture is generally less than the *in situ* σ_3 and consequently less than the pressure needed for hydraulic fracturing if the fracture is favorably oriented for shearing, that is, if the fracture makes an angle of about 30° with the maximum principal stress σ_1 (Pine & Batchelor 1984). It is also assumed that dilation associated with shear failure, owing to the roughness and irregularity of the fracture surface, leads to a permanent gain of aperture and fracture permeability, a mechanism referred to as self-propping (Hsiung *et al.* 2005).

Taking into account the above theoretical aspects, the injection of pressurized fluid for hydraulic fracturing and/or hydraulic shearing will lead to different geometries depending on the tectonic regime. According to Anderson's (1951) classification of tectonic regimes, a thrust-fault (TF) regime is characterized by a vertical σ_3, and horizontal σ_1 and σ_2, referring to the minor, major, and intermediate principal stresses, respectively. In such an environment, hydraulic treatments will promote the creation and enhancement of structures with horizontal and subhorizontal geometries (Jeffrey *et al.* 2009; Bendall *et al.* 2014). Normal-fault (NF) regimes involve a vertical σ_1 and horizontal σ_2 and σ_3, and strike-slip (SS) regimes are characterized by a vertical σ_2 and horizontal σ_1 and σ_3. In both regimes, hydraulic treatments will therefore promote the creation/reactivation of vertical and subvertical discontinuities (Evans *et al.* 2005; Häring *et al.* 2008). Such considerations imply that, theoretically, horizontal boreholes can affect a larger rock volume in NF and SS regimes, whereas in TF regimes vertical boreholes could affect a larger volume.

The optimal deployment of hydraulic fracturing and stimulation is impaired because our understanding of the key processes involved, including hydromechanical coupling in fractured rock and the associated generation of seismicity, is still poorly understood (Jung 2013; Kaiser *et al.* 2013). This limits our ability to design and optimize reservoir enhancement operations and to mitigate any environmental impact on groundwater quality and induced seismicity associated with rock mass response, that is, slip and tensile opening of fractures (Dusseault & McLennan 2011; Fairhurst 2013; Vincent 2013). Despite different geological settings, rock properties, local site conditions, and operational objectives, the ability to develop connected rock mass permeability by means of hydraulic treatments is a shared challenge faced by enhanced geothermal systems (EGS), shale gas, and deep mining projects. In EGS, the enhancement of permeability at depth is necessary for initiating long-term circulation of water between an injection and a pumping well at volumetric flow rates and temperatures of commercial interest, that is, >80–100 l s^{-1} at 200°C (Evans *et al.* 2005; Polski *et al.* 2008). This enhancement should preferably occur across a large volume and multiple fractures distributed throughout the reservoir to ensure an optimal exchange of heat between the rock

and the fluid, as well as to avoid a rapid deterioration of reservoir permeability if major flowing fractures are clogged by mineral precipitation. In shale gas, the development of connected permeability is necessary for enhancing well productivity and maximizing resource recovery in tight reservoir rocks. Similar issues arise regarding closure or collapse of induced fractures leading to rapid deterioration of reservoir permeability and declining well production. In the mining industry, increased fracture connectivity is also of interest, especially for increased fragmentation with use of the block caving mining method (Araneda *et al.* 2007). Another issue facing deep mines with the targeting of deeper ore bodies is the management of high stresses and associated hazards, such as rock bursting. One of the primary current research objectives is to verify the capacity to modify the stress field prior to mining by means of fluid injection and induced hydraulic shearing (HS). Reactivation of natural fractures via hydraulic shear/slip has the potential to relax local concentrations of stress and mitigate related ground-control hazards (Kaiser *et al.* 2013). However, the effectiveness of a HS injection relies on the presence of sufficient connected permeability to allow the diffusion of fluid pressure. These permeable paths are fewer and poorly connected in massive crystalline rocks where many deep mines are located, and must first be generated.

In this context, a series of hydraulic fracturing (HF) and hydraulic shearing (HS) injection experiments are planned to be carried out in a deep mine in New South Wales, Australia. Extensive monitoring of the rock mass response will be carried out, including microseismicity, stress change, and tilt deformations. The injections will be designed to test two central hypotheses: (i) HF and/or HS can be promoted by adjusting fluid injection parameters; (ii) HF and/or HS can permanently modify the rock mass properties. Indeed, HF alone does not generate significant permanent changes in permeability or stress because of the narrow zone of influence and closure of aperture and asperity locking after injection ceases. Permanent changes in rock mass permeability/stress can be achieved through HS by causing slip and dilation along natural fractures, possibly aided by injecting a strength-reducing agent (low friction grout). Installation of the monitoring network has been completed with the injection sequences scheduled to begin in late 2014. A detailed site and experiment description can be found in Kaiser *et al.* (2013). This experiment will produce data under field-scale conditions on the following: (i) stress field modification/relaxation, (ii) rock mass deformation, (iii) induced seismicity, and (iv) increasing rock mass fragmentation and permeability. The experiment will consist of multiple injections with varying flow rates, injection interval lengths (promoting HF and HS), and absence or presence of stress shadows from earlier adjacent injections.

This paper reports the findings from a detailed set of numerical models performed as part of the experiment design. These analyses have been used to help define the fluid injection magnitudes and rates, optimal locations of monitoring sensors, and preliminary estimates of expected response (magnitude and sensitivity analyses). Specifically, these models aim to investigate and quantify the capacity to develop interconnected permeability via different designs of fluid injection in deep, massive, crystalline rocks populated by a poorly connected network of natural fractures. Focus is also placed on investigating the dominant hydromechanical processes promoting or inhibiting the development of permeability, by comparing the numerical outcomes with past field experiments focusing on the development of permeability. This quantification issue has not been addressed by previous numerical modeling studies.

The paper is organized in three parts as follows: the first introduces the numerical approach; the second focuses on field properties, modeling strategy, and design; and the third presents the results and discussion of their interpretation.

NUMERICAL APPROACH

Currently, no modeling approach is readily available that fully captures all aspects of the hydromechanically coupled processes involved in hydraulic fracture initiation, propagation, and interaction with pre-existing natural fractures. As our focus is the development of interconnected permeability in a fractured rock mass in response to hydraulic fracturing and hydraulic shearing injections, the fully coupled hydromechanical distinct-element code UDEC (Itasca 2013) was selected because of its ability to capture in detail the governing mechanisms: (i) the tensile and shear response of a natural discrete fracture network (DFN) to fluid pressure changes and (ii) the relevant physical processes related to the hydromechanical response of flow in fractures (Miller 2015). Within this context, thermal and chemical couplings are neglected. A key advantage of using UDEC is that it allows for the explicit modeling of an invaded zone (Dusseault & McLennan 2011) ahead and around a hydraulic fracture, together with tensile opening of pre-existing natural fractures favorably oriented for HF (i.e., orthogonal to σ_3) and tensile breakage of intact rock bridges represented by preferential paths of weakness (referred to here as incipient fractures; Fig. 1).

The main limitation of the chosen numerical technique is that the blocks comprising the problem domain are indivisible once time stepping begins; accordingly, hydraulic fracture propagation is limited to the predefined DFN. To mitigate this, strength properties are assigned to segments of the fracture network to represent either pre-existing natural fractures or intact rock bridges (incipient fractures), thus providing the necessary degrees of freedom for the propagation of a hydraulic fracture (Zangeneh *et al.*

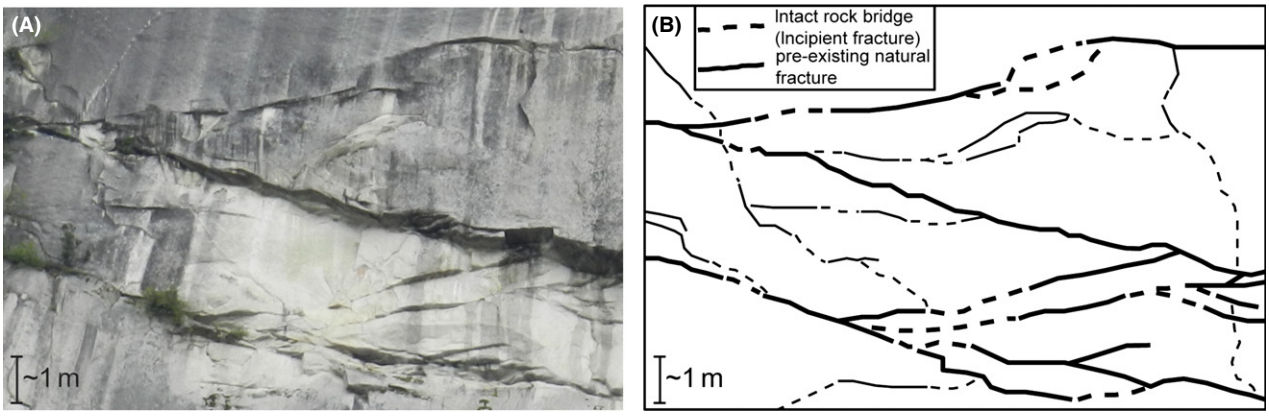

Fig. 1. (A) Picture showing a fractured crystalline rock mass (British Columbia, Canada) and (B) its illustrative conceptualization as a fracture network composed of cohesionless natural pre-existing fractures interconnected with intact rock bridges behaving as preferential paths of weakness (incipient fractures).

2012). The network is defined through the vertices of randomly sized polygonal blocks generated via a Voronoi tessellation discretization scheme. This algorithm arbitrarily distributes a set of points within the domain of discretization that are then moved iteratively until reaching a uniform spacing, to which Voronoi polygons are fitted (Itasca 2013). It should be noted that the Voronoi approach increases the computational time of a coupled hydromechanical analysis. Moreover, Voronoi blocks include a large number of segments that will be perpendicular to the major principal stress, effectively stopping the hydraulic fracture from propagating further by forcing it to open against the major principal stress.

To overcome this limitation, an alternative approach was developed for this study consisting of 'directional polygons'. These control the direction of incipient fractures so that fracture propagation directions, that is, intact rock bridges between adjacent nonpersistent (stopping against a rock block), nonconnected, pre-existing natural fractures, align at a favorable orientation for fracture initiation (±15–30 degrees relative to σ_3), in contrast to the random directions resulting from the Voronoi tessellation. This work simulates a fully coupled hydromechanical analysis at field scale, that is, greater than one hundred meters and incorporating a detailed fracture network geometry. To date, these types of distinct-element models are intractable in 3D and can only be practically achieved through 2D analyses.

EXPERIMENT AND NUMERICAL ANALYSIS DESCRIPTION

Geological setting

The experiment design was performed for the case of injection at depths between 1400 and 1430 m within a sparsely fractured (massive) monzonite. Mapping observations made in an access tunnel, and in other parts of the mine, indicate that the natural fracture network is weakly interconnected and consists of three main fracture families plus some random orientations as shown in Table 1. The stress state at the site was determined by multiple overcoring stress measurements and back analyses of excavation performance. These indicate a thrust regime where the major and intermediate principal stresses, σ_1 and σ_2, are horizontal and the minor principal stress, σ_3, is vertical. The horizontal to vertical stress ratio, K, is approximately 1.7. The rock mass is assumed to be under zero initial pore pressures, in accordance with field observations. No information is available on initial fracture apertures. However, based on the *in situ* stress state, fracture families 1 and 2 should initially be tightly closed and fracture family 3 more open because it is more orthogonal to σ_1. A series of development tunnels and niches provide access to install the monitoring network, together with a vertical 96-mm-diameter borehole that will be used to inject fluids following a schedule alternating between hydraulic fracturing (HF) and hydraulic shearing (HS) treatments. Several observation boreholes will be used to complete the monitoring network and to directly observe HF and HS fracture responses intersecting the boreholes.

Injection intervals and volumetric flow rates proposed below are our starting strategy for inducing dominant HF or dominant HS within the rock. One of the objectives of the modeling exercise is to assess whether they will likely lead to the desired rock mass response. The injection design adopts current HF practices at the site, that is, injection within a small-packed interval of 2 m into which a volumetric flow rate of 400 l min^{-1} will be pumped to exceed the breakdown pressure and initiate a new tensile hydraulic fracture. The use of HS has not yet been explored at the site; thus, the optimal conditions in this case are uncertain. Injection metrics for HS include a larger packed interval (15–30 m) and a lower injection rate, <250 l min^{-1}. These are based on the assumption that to achieve HS without HF, the injection interval must be long enough to straddle

Table 1 Field data and parametric inputs used in numerical models.

Discrete fracture network (DFN)				
	Dip direction [degrees]	Dip angle [degrees]		
Family 1	035	85		
Family 2	340	80		
Family 3	260	15		
Intersection between DFN and the 2D vertical model oriented E–W				
	Dip direction [degrees]	Dip angle [degrees]	Spacing [m]	
Family 1	090	81	2.4	
Family 2	270	63	3.6	
Family 3	270	15	4.2	
Persistence of fractures: fully or variable (see Fig. 2)				
Rock properties		**Fracture properties**		
Young modulus E [Pa]	60×10^9		Incipient	Natural
Poisson ratio ν [-]	0.25	Normal stiffness k_n [Pa m^{-1}]	1.3×10^{11}	1.3×10^{11}
Density ρ [kg m^{-3}]	2700	Shear stiffness k_s [Pa m^{-1}]	1.3×10^{10}	1.3×10^{10}
Bulk modulus K [Pa]	$K(E, \nu)$	Tensile strength T [Pa]	0.5×10^6	0.0
Shear modulus G [Pa]	$G(E, \nu)$	Cohesion C [Pa]	1.0×10^6	0.0
Fluid properties and constants		Friction angle Φ [°]	30	45
Viscosity μ [Pa s]	0.001	Aperture at zero effective normal stress a_0 [m]	2.0×10^{-5}	2.0×10^{-5}
Density ρ_w [kg m^{-3}]	1000	Residual aperture a_{res} [m]	4.0×10^{-6}	4.0×10^{-6}
Bulk modulus K_w [Pa]	0.1×10^9	Dilation angle ψ [degrees]	0	0
Gravity g [m s^{-2}]	9.81			
***In situ* stress state**				
Stress σ [MPa], depth Z [m]	Orientation			
$\sigma_1 = 5 + 0.0479\ Z$	Horizontal E-W			
$\sigma_2 = 0 + 0.0344\ Z$	Horizontal N-S			
$\sigma_3 = 0 + 0.0297\ Z$	Vertical			

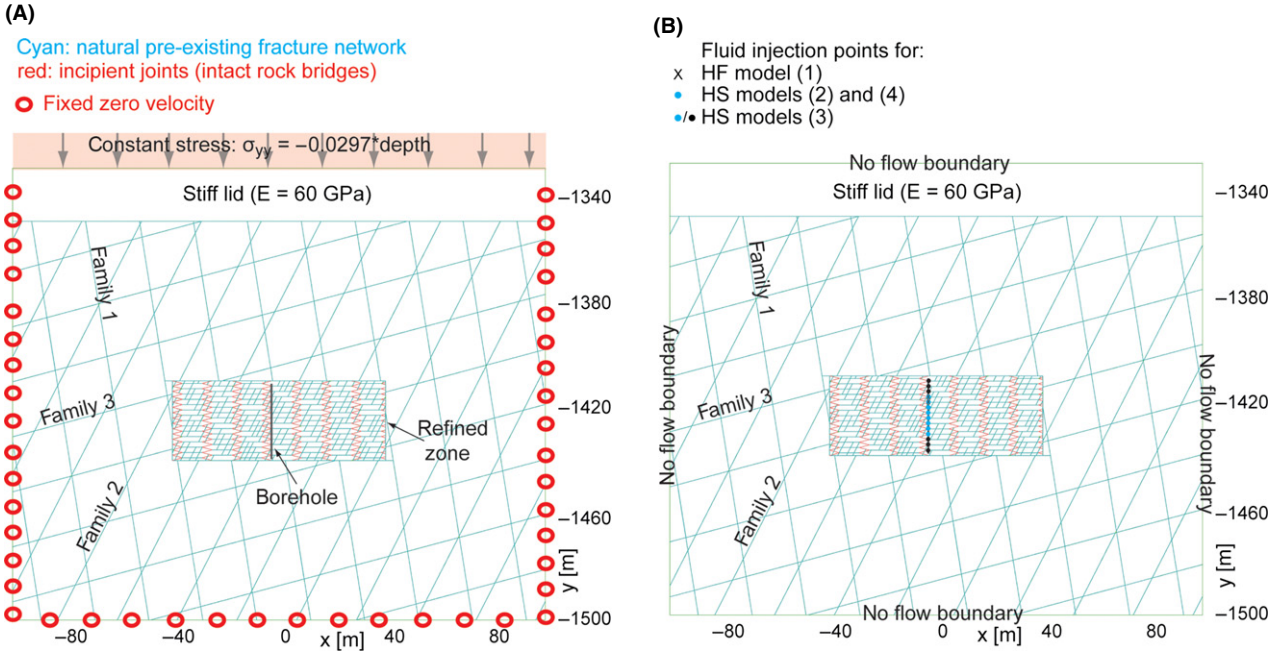

Fig. 2. (A) Mechanical and (B) hydraulic boundary conditions with the model geometry and fracture network implementation. Refer to Figs 3 and 5 for an enlargement of the refined zone.

several multiple natural fractures and the injected flow rate must be controlled so that the pressure in the borehole is kept below σ_3. The injection design also includes consideration of logistical and equipment constraints.

Modeling strategy

As previously stated, modeling of hydraulic fracturing was carried out to explicitly represent a discrete fracture network composed of the following: (i) natural pre-existing cohesionless fractures superimposed on top of (ii) incipient fractures behaving as intact rock bridges and having intact rock properties. In UDEC, the transient flow equation for a compressible fluid is fully coupled with kinematic equations for a discontinuum medium. In such a case, the breakage of an incipient fracture or the slipping of a natural fracture under increasing pore pressure depends not only on Eqs 1 and 2, but also on the entire deformation response of the fractured rock mass, including rotation, wedging, and elastic strain of the intact rock blocks as well as the opening/closure and slip along the segments of the fracture network. A linear elastic constitutive model and an elasto-plastic Coulomb slip model are applied to the rock blocks and fractures, respectively.

Pore pressure propagation through the fracture network is modeled using nonlinear stress-dependent fracture aperture. Once a natural or an incipient fracture slips or opens in response to the disturbed stress field, fluid flow and pressure diffusion take place conforming to the cubic law (Whiterspoon *et al.* 1980)

$$Q = \frac{a^3}{12}\frac{\rho_f g}{\mu_f}\nabla H \tag{3}$$

where Q is the flow rate parallel to the fracture, a is the fracture hydraulic aperture, ρ_f is fluid density, g is gravitational acceleration, μ_f is the fluid viscosity, and ∇H is the hydraulic head gradient. In Eq. 3, the fracture is conceptualized as a pair of parallel surfaces whose orthogonal distance corresponds to the hydraulic aperture a. In this model, the hydraulic aperture matches the mechanical aperture and results in a parallel fracture permeability and transmissivity of $k = a^2/12$ and $t_f = a^3/12$, respectively. The aperture and parallel fracture permeability are controlled by the following hydromechanical processes: (i) pore pressure effects, where changes in pore pressures (effective stresses) result in a mechanical deformation affecting fracture aperture and permeability; (ii) stress transfer, where a change in applied stresses results in a change in fluid pressure and stiffness. Depending on the magnitude of these two processes, fracture aperture will vary linearly between a residual hydraulic aperture a_{res}, a hydraulic aperture at zero normal effective stress a_0, and optionally, a maximum hydraulic aperture a_{max}; finally, (iii) hydraulic shearing, accompanied by the permanent opening of the fracture controlled by the dilation angle specified (Itasca 2013). Note that in this work, rock blocks are considered to be impervious and flow only occurs in the fractures.

Due to the accuracy of the governing algorithms, the analysis of hydromechanical processes is time-consuming and becomes intractable at large scales, in 3D, and for long fluid flow times; one minute of injection time for a field-scale model can take up to one day of computation time on an Intel i7 3.2 GHz machine with 64 GB of RAM. Given that hydraulic fractures propagate orthogonal to σ_3 the use of the directional polygon discretization technique developed here and shown in Fig. 2 lends itself to more efficient solution times compared to the random orientations derived from using UDEC Voronoi. For large-scale models, that is hundreds of meters or greater, another means to reduce computation time is to separate the mesh into refined and nonrefined zones. The refined zone is designated around the injection well and along the expected path of the hydraulic fracture and invaded zone, incorporating the network of pre-existing natural fractures and intact rock bridges. The nonrefined zone helps to extend the model boundaries away from the zone of interest and allows for the investigation of the large-scale mechanical response (strain field) of the fractured rock mass.

Model geometry and mechanical conditions

Figure 2 and Table 1 summarize information described in this section. The 2D model corresponds to a vertical slice 200 m wide and 170 m high in the σ_1-σ_3 plane oriented east–west with a refined zone 80 × 30 m in the middle, and a stiff cover/beam along the top of the problem domain. This stiff cover is used in conjunction with a constant stress condition assigned along the top of the model to add a bending stiffness to this boundary, simulating the influence of more than 1300 m of overburden above the modeled domain. Rollers (zero normal displacement) are specified for the remaining boundaries. The lateral boundaries are restricted in the x-direction and the bottom boundary restricted in the y-direction. The *in situ* stress state is compressive with a major principal stress σ_1 (horizontal) of 73 MPa and a minor principal stress σ_3 (vertical) of 42 MPa at the level of the injection (1412 m depth). The *in situ* stress state is imposed to increase linearly with depth according to the equations presented in Table 1.

The introduction of fractures in the model requires a compromise between the desire to capture the disconnected nature and approximate geometry of the natural fracture network at the site and the need to minimize complexity and associated computation times. Initially, the three fracture families mapped in the mine tunnels are considered for implementation in the model by computing their intersection with the vertical model plane (see

Table 1). In the refined zone, the disconnected nature of the fracture network is represented by inserting nonpersistent horizontal fractures (approximating fracture family 3) connected via intact rock bridges (incipient fractures) dipping at 15 degrees. These two elements form the main fabric of the model on which a west dipping set (representing family 2) is added. Family 1, which is subvertical and perpendicular to σ_1, is omitted because it is unfavorably oriented, highly compressed, and will not respond to the fluid injection (i.e., open against σ_1). This simplification helps to reduce computational time and avoids numerical problems related to excessive fluid stiffness when subject to substantial compression. The limitations of the modeled geometry are that: (i) the horizontal fractures forming the main fabric of the model are exactly aligned with the principal stress axis, reducing the ability for these fractures to shear (hydroshear), and (ii) the rock bridges are geometrically aligned, potentially forming a barrier to fracture propagation. The implications of these limitations will be discussed in the results section of this paper. In the nonrefined zone, the discrete fracture network (DFN) is introduced by considering persistent cohesionless fractures having a spacing of 20 m. Across the entire model domain, the rock blocks are modeled as being elastic.

Fluid injection and hydraulic conditions

Fluid injection is simulated by specifying a constant volumetric flow rate entering the model at points where the vertical borehole intercepts the fracture network. The borehole itself and the associated stress perturbation are not included in this model. Four injection designs are tested as follows: HF model (1) includes simulation of 400 l min^{-1} injected over a 2-m packed interval for 60 min; HS model (2) includes simulation of 50 l min^{-1} injected over a 15-m packed interval for 90 min; HS model (3) includes simulation of 50 l min^{-1} injected over a 30-m packed interval for 90 min; and HS model (4) includes simulation of 250 l min^{-1} injected over a 15-m packed interval for 90 min. HF model (1) mainly focuses on the capacity to develop interconnected permeability by means of tensile hydraulic fractures. The HS models mainly focus on the capacity to enhance interconnected permeability by means of hydraulic shearing. The fluid injections are simulated with full consideration given to the logistical and equipment constraints at the mine. As previously noted, computational constraints limit the length of the injection times modeled to those <120 minutes. Nevertheless, these still allow the governing hydromechanical processes to be captured and are considered to be representative of longer injections (i.e., several hours to days).

Applied injection rates need to be scaled from 3D to 2D according to

$$Q_{2D} = Q_{3D}\,\alpha \tag{4}$$

where Q_{2D} stands for the scaled injection rate in $m^3\ s^{-1}\ m^{-1}$, Q_{3D} is the volumetric injection rate, and α is a scaling reduction factor. The value of α depends almost exclusively on two points as follows: (i) the scaling from 3D to 2D and (ii) the anisotropy of fluid flow in fractured rocks due to *in situ* stress and the intrinsic properties of the natural fractures network. In 3D, volumetric fluid injection is commonly considered as a radial process. A 3D radial process cannot be scaled to a 2D vertical configuration. There is thus no clear solution for deriving α. A parametric analysis was carried out retuning a value of 1/70, which was subsequently assigned to all injection metrics. This value yields hydraulic fracture lengths which are in agreement with those observed during preconditioning treatments at the mine. Note that $\alpha = 1/70$ is specific to the stress environment of field study site and to the model size. Note also that despite the scaling injection rates and 2D nature of the model, for practical purposes, the model input and output will be expressed in volumetric terms, that is, l min^{-1} and m^3, throughout the paper.

No flow boundaries surround the model, and the rock mass is under zero initial pore pressures throughout the model. This agrees with field observations. The fluid properties correspond to water, except for the bulk modulus which is one order of magnitude lower than standard values for water. This lower bulk modulus allows for the consideration of small changes in fluid volume if subjected to high stress, thus avoiding numerical instabilities related to an excessive fluid stiffness. The lower bulk modulus also works to slightly decrease computational times. Note that the contribution of the bulk modulus of the fluid is almost irrelevant with regard to the pressure diffusion and fluid penetration distances. These depend mainly on the failure of fractures and rock mass deformation. Again, rock blocks are considered impervious, and unsaturated flow processes are neglected. This is justified by the fact that water can only flow after rupture events, implying that generated pore space is instantaneously saturated. After the injection phase, backflow to the wellbore is simulated by specifying a constant fluid pressure in the borehole.

Parametric inputs

Parametric inputs are based on field data, literature values, and personal communications with mine staff (see Table 1). Initial fracture apertures are in the order of tens of micrometers, which is reasonable for such depths and stresses (e.g., see Snow 1970; Luthi & Souhaité 1990). UDEC considers a fracture as open when its strength is exceeded or the fracture has slipped (Itasca 2013). Model results are considered here to be acceptable as long as the hydraulic fractures generated and corresponding fluid flow remains limited to the refined zone.

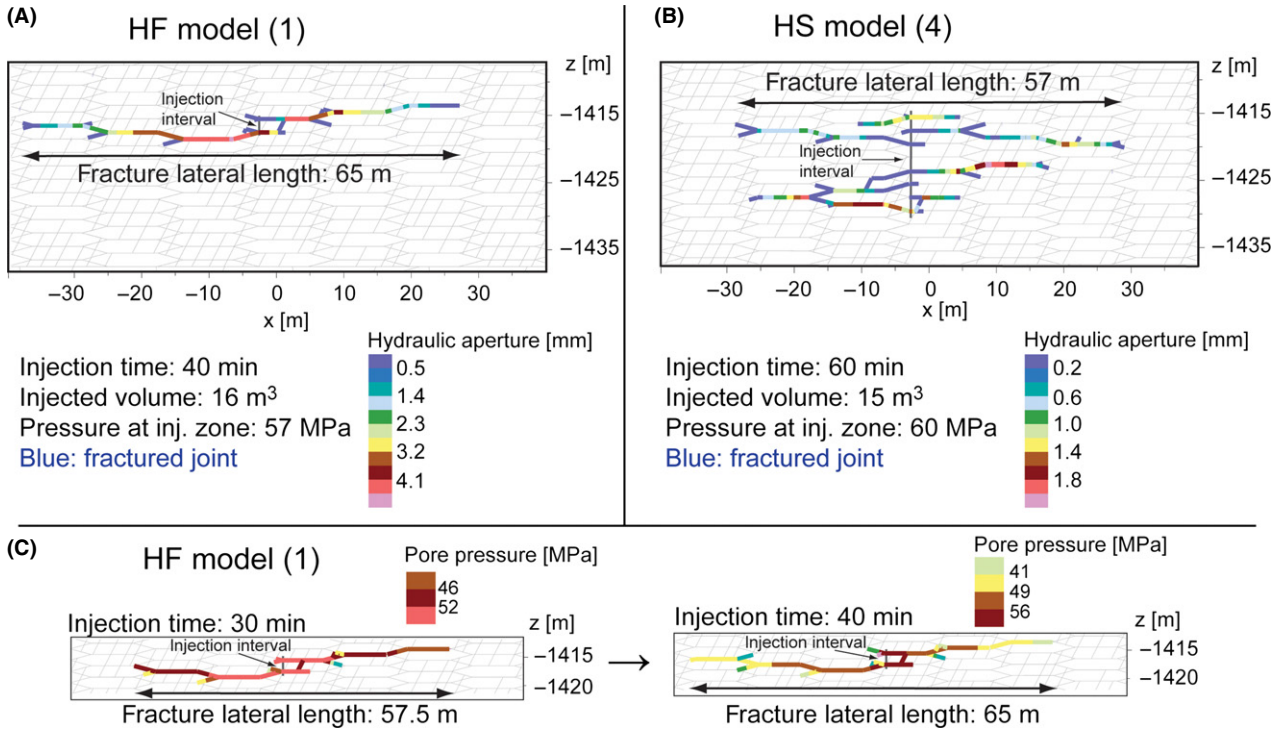

Fig. 3. Model enlargements showing total lateral extent and opening of hydraulic fractures for (A) hydraulic fracturing model (1) after 40 min of fluid injection at 400 l min^{-1} into a 2-m packed interval, and (B) hydraulic shearing model (4) after 60 min of fluid injection at 250 l min^{-1} into a 15-m packed interval. (C) Cyclical increase and decrease of pore pressures accompanying hydraulic fractures growth.

RESULTS

Growth, persistence, and aperture of hydraulic fractures

Length and shape

As expected, for HF model (1), hydraulic fractures grow orthogonal to σ_3 along a path linking horizontal pre-existing cohesionless fractures and failed subhorizontal rock bridges. After an injected volume of 16 m^3 (40 min of injection at 400 l min^{-1}), hydraulic fractures reach a total lateral extent of 65 m (Fig. 3A). This agrees with previous observations of hydraulic fractures generated at the study site (Bunger *et al.* 2011), providing a measure of model validation and confirming that the input parameters are reasonable.

Incipient fractures (intact rock bridges) first slip and then are broken in tension. Horizontal natural fractures are opened normal to the horizontal plane. Only one fracture belonging to family 2 (steeply dipping to the west) is activated, close to the injection point. The largest hydraulic apertures, in the range of millimeters, occur close to the injection well and progressively decrease toward the tip of the hydraulic fracture. Fracture growth occurs both toward the east (model right) and west (model left). The most important observation emerging from Fig. 3A is that the developing hydraulic fracture remains constrained within a quasi-planar geometry and does not develop additional branches. A similar behavior holds for the HS models (Fig. 3B), where out of the seven branches activated along the wider injection interval, only three branches (two to the west and one to the east) continue at some distance from the well with others converging and merging. This observation is in agreement with laboratory results from Bunger *et al.* (2011). A plausible explanation for this behavior is that tensile opening of a hydraulic fracture increases the confining stresses seen by the adjacent branches (stress transfer/shadowing), limiting/arresting their development. This mechanism could also explain observations from hydraulic stimulation tests related to enhanced geothermal systems, where different lengths of packed intervals have led to the propagation of only a few fractures instead of a pervasive stimulation of a rock mass volume (Jung 2013). However, an alternate explanation involving the influence of the pre-existing permeability field could also be invoked (Evans *et al.* 2005).

Pressure–time response and cyclic growth

Figure 3C shows the pore pressure behavior during hydraulic fracture growth. Before a failure event, pore pressure increases, leading to decreasing pressure gradients and flow velocities between the well and hydraulic fracture fronts. Beyond the front, the pressure gradient is high, but flow is null due to the very low permeability of the incipient fractures before failure. Failure happens when pore

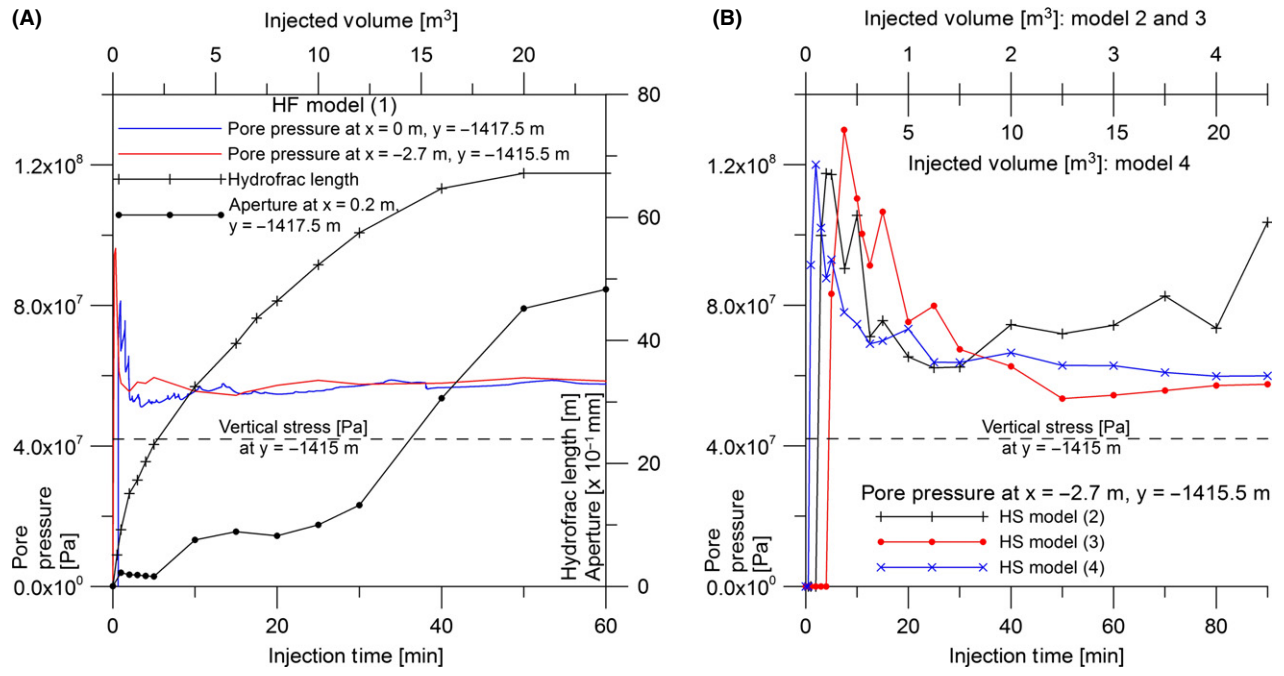

Fig. 4. (A) Pore pressure at and close to injection, hydraulic fracture length, and aperture as a function of injection time and volume (in m^3) for hydraulic fracturing (HF) model (1): 400 min^{-1} into a 2-m interval. (B) Pressure–time response for hydraulic shearing (HS) models at injection point $x = -2.7$ m, $y = -1415.5$ m; HS model (2): 50 l min^{-1} into a 15-m packed interval; HS model (3): 50 min^{-1} into a 30-m packed interval; HS model (4): 250 l min^{-1} into a 15-m interval.

pressures at the hydraulic fracture front exceed the incipient/natural discontinuity strength leading to increasing fracture volume and permeability. This allows fluid flow and the release of accumulated pore pressures, leading to increasing pressure gradients and flow velocities between the injection well and hydraulic fracture fronts. This sequence repeats itself in a cyclical manner as indicated by the repeating peaks in the blue pore pressure curve of Fig. 4A. The process is much more pronounced at early stages of injection because initiation (first breakages) coincides with a shorter hydraulic fracture length and therefore limited system compliance. This cyclic growth of hydraulic fractures is supported by microseismic signals recorded during hydraulic fracturing (Eaton *et al.* 2014). Unfortunately, in Fig. 4A, the resolution of the model output tracking hydraulic fracture growth with injection time is too low compared to that for the pore pressure response, and the growth cannot be directly related to each pore pressure peak. Early stages of injection are also characterized by rapid growth of the fracture. Propagation velocity decreases as the fracture enlarges. This is primarily because the pore pressure gradient between the wellbore and hydraulic fracture front decreases with increasing fracture length. Thus, it becomes increasingly more difficult to increase pore pressure at the fracture front and exceed the fracture tip rock strength. In contrast, the hydraulic fracture aperture profile indicates that as the hydraulic fracture develops laterally, it is harder to open. Thus, the hydraulic fracture begins to open considerably only when the growth decelerates and pressures increase. It is important to note that these normal dislocations are fully reversible due to the elasticity of fractures if slip and dilation do not occur (Tsang & Witherspoon 1981; Cappa 2006; Preisig *et al.* 2012). Thus, if pore pressure is significantly decreased after injection, the aperture of the hydraulic fracture is much reduced. A phase of proppant injection, comprised of fluid and sand, is commonly employed to avoid elastic closure of hydraulic fractures and ensure permanent apertures.

Figure 4 shows pore pressure as a function of injection time and volume. In all cases, there is a substantial build up of pore pressure related to the initial impervious character of the massive rock, regardless of injection design. For HF model (1), compared to the HS models, the pressure build up is more rapid because of the higher injection rate. After this peak, the pore pressure stabilizes around 55 MPa. The cyclical increase and decrease of pore pressure with hydraulic fracture growth is then responsible for localized pore pressure peaks. In Fig. 4, it is also interesting to note that the increase of packed injection interval length leads to increasing pressure build up; see the HS models compared to the HF model and/or the HS model (3) compared to the HS models (2)/(4). In fact, even for the HS models, tensile opening dominates, regardless of the injection design, principally because of the fracture net-

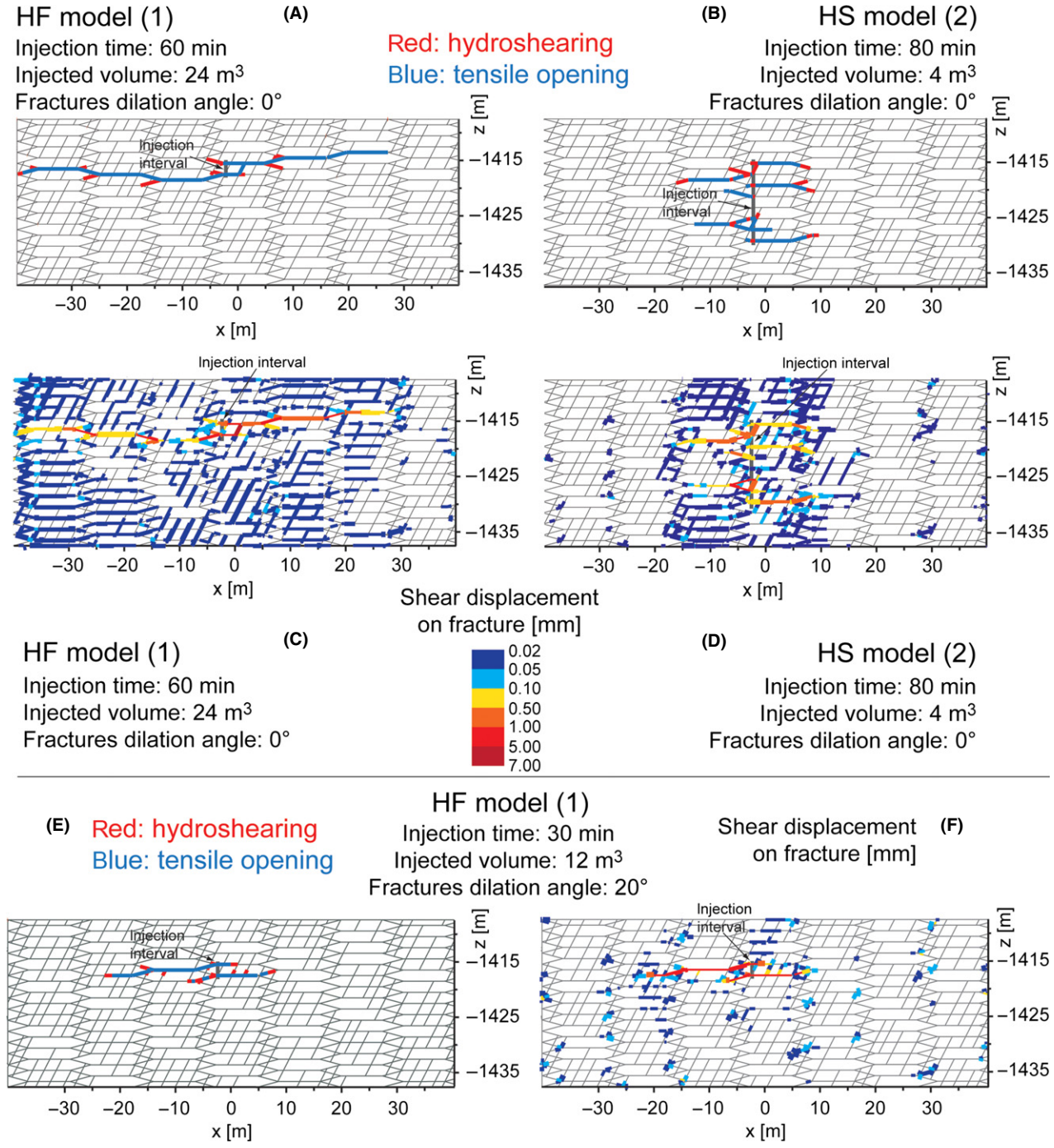

Fig. 5. Model enlargements illustrating hydroshear/slip and tensile opening and shear displacement on fractures for (A)–(C) hydraulic fracturing (HF) model (1) after 60 min of fluid injection at 400 min^{-1} into a 2-m packed interval, (B)–(D) hydraulic shearing model (2) after 80 min of fluid injection at 50 l min^{-1} into a 15-m packed interval, and (E)–(F) HF model (1) after 30 min of fluid injection with fractures having nonzero dilation angle. Note that for shear displacement, fracture line thickness increases when its value is close to the upper boundary of its color grade.

work geometry and parametric inputs (Fig. 5D). Thus, the increase of packed interval length results in an increasing number of natural and incipient fractures opening and breaking, leading to interaction between fractures in the form of stress transfer/shadows. This increases the normal stresses acting on the adjacent fracture planes, which results in local increases in fracture strength. As soon as the hydraulic fractures initiate and begin to develop, pore pressures are consequently decreased. This pressure behavior is not realistic compared to that observed in major hydraulic stimulation tests for EGS (Evans *et al.* 2005; Häring *et al.* 2008), because the modeled injection

is performed via different points. However, this behavior clearly illustrates the influence of stress transfer during the injection.

Shear displacements on fractures

As previously noted, tensile breakage of the incipient fractures may be preceded by the shear slip. However, for all models, this is largely the major manifestation of shearing directly related to the pressure perturbation induced by the injection (Fig. 5A,B). In fact, shear displacements on natural pre-existing fractures of family 2 mainly occur as a consequence of movement and rotation of rock blocks (Fig. 5C,D), related to sinistral or dextral shear movement between the tensile hydraulic fractures. The weak presence of hydroshearing is explained by the absence of favorably oriented long-persistent fractures, the input parameters selected, that is, zero dilation angle, and the stress transfer accompanying tensile opening, which increases the confining stress acting across the neighboring fractures, reducing their ability to slip. Despite the effort to promote more hydroshear events by changing the injection design in the HS models, long fractures favorably oriented for hydroshearing are sparse in the refined zone. Moreover, the natural rock mass conditions are considered to be impermeable, thus preventing pressure diffusion, and implying that the rock must first be fractured. Nevertheless, the models show that the first rupture events are associated with pressure build up developing along the incipient and pre-existing subhorizontal fractures nearest the injection. Then, as the initiated hydraulic fractures advance and permeable paths develop, pore pressures also begin to diffuse into the subvertical fractures of family 2.

Figure 5E,F illustrates the response when a high dilation angle is applied ($\psi = 20°$). Subvertical fractures of family 2 fail in shear when pressurized (Fig. 5E). However, hydroshear is rapidly inhibited along these fractures because they are not sufficiently persistent, and because of the increasing shear strength associated with fracture dilation and stress transfer. No remarkable gain in fracture connectivity occurs for the high dilation angle case, and tensile opening remains the dominant process. These results confirm previous observations that shear displacement and associated gain in permeability through hydroshearing require the presence of natural fractures sufficiently long and favorably oriented within the stress field (Rutqvist 2015). Fig. 5E,F also shows that the addition of a dilation angle has resulted in hydraulic fracture paths that differ slightly compared to the case with a zero dilation angle (Fig. 5A). Regardless of the dilation angle assumed, the geometry of the fractured zone still reflects the pre-existing stress field and fracture network.

Impact on the rock mass

Rock mass deformation

Tensile opening of horizontal hydraulic fractures results in vertical compressive strain of the adjacent fractured rock, with the highest displacement vectors being close to the injection zone (Fig. 6A). These deformations are partly attenuated by elastic deformation of the rock blocks, leading to lower displacements away from the hydraulic fracture. Despite this, the upper boundary is still subject to millimeter scale uplift and bending. The displacement field presented in Fig. 6A for HF model (1) is vertically asymmetric, with a highly attenuated zone below the hydraulic fracture due to the fixed bottom boundary condition. Note that a slight vertical asymmetry is also expected due to the increase of *in situ* stresses with depth. Deformation of the

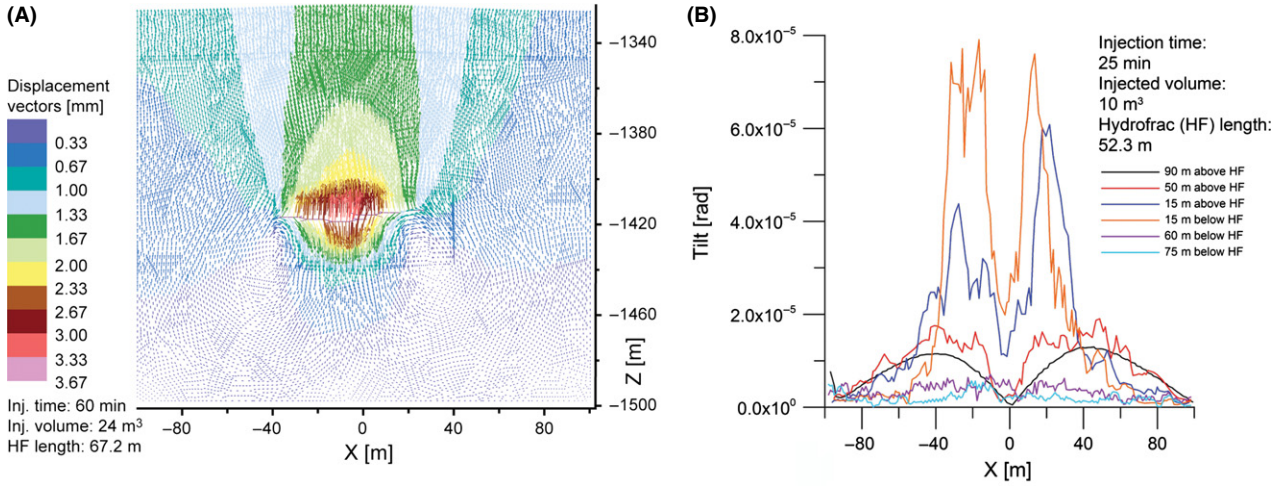

Fig. 6. Hydraulic fracturing model (1): induced (A) displacement field after 60 min of fluid injection at 400 l min^{-1} into a 2-m packed interval and (B) tilt after 25 min of fluid injection for 6 observation planes located above and below hydraulic fractures.

fractured rock mass under fluid injection also results in strains and block rotation, which induces tilt relative to a horizontal plane. Not surprisingly, the highest tilt magnitudes occur close to the injection zone and decrease along the vertical axis (Fig. 6B). Again, there is a strong vertical asymmetry between tilts located above and below the hydraulic fracture. The weak horizontal asymmetry results from the difference in shape between the hydraulic fracture propagating eastward and westward. In Fig. 6B, another important observation is that the location of maximum tilt is laterally offset from the center of the hydraulic fracture, and this offset increases with vertical distance away from the fracture.

Stress change

Tensile opening of horizontal hydraulic fractures under fluid injection leads to vertical strains, and accordingly, increasing vertical stresses above and below the hydraulic fracture. In contrast, at the tips of the hydraulic fractures, vertical opening results in decreasing stresses (Fig. 7C–F). This overall behavior is partly due to the horizontal orientation of the major principal stress, as well as a Poisson's ratio effect where the vertical shortening strains adjacent to the hydraulic fracture produce expanding strains in the horizontal direction and therefore increased horizontal stresses (Fig. 7A–D). The change in shear stress illustrated in Fig. 7B–E reflects the general right-lateral shear displacement affecting the system. Note that for the HS models, the shape of change in stresses is similar to that presented in Fig. 7 for the HF model.

On the one hand, the increase of stress above and below the primary hydraulic fractures leads to a stress shadow/transfer around the adjacent pre-existing and incipient fractures, limiting their possibility to slip or open. On the other hand, the decrease of stress at the hydraulic fracture tip fronts creates a preferential path, allowing the hydraulic fracture to continue propagating far away from the injection zone.

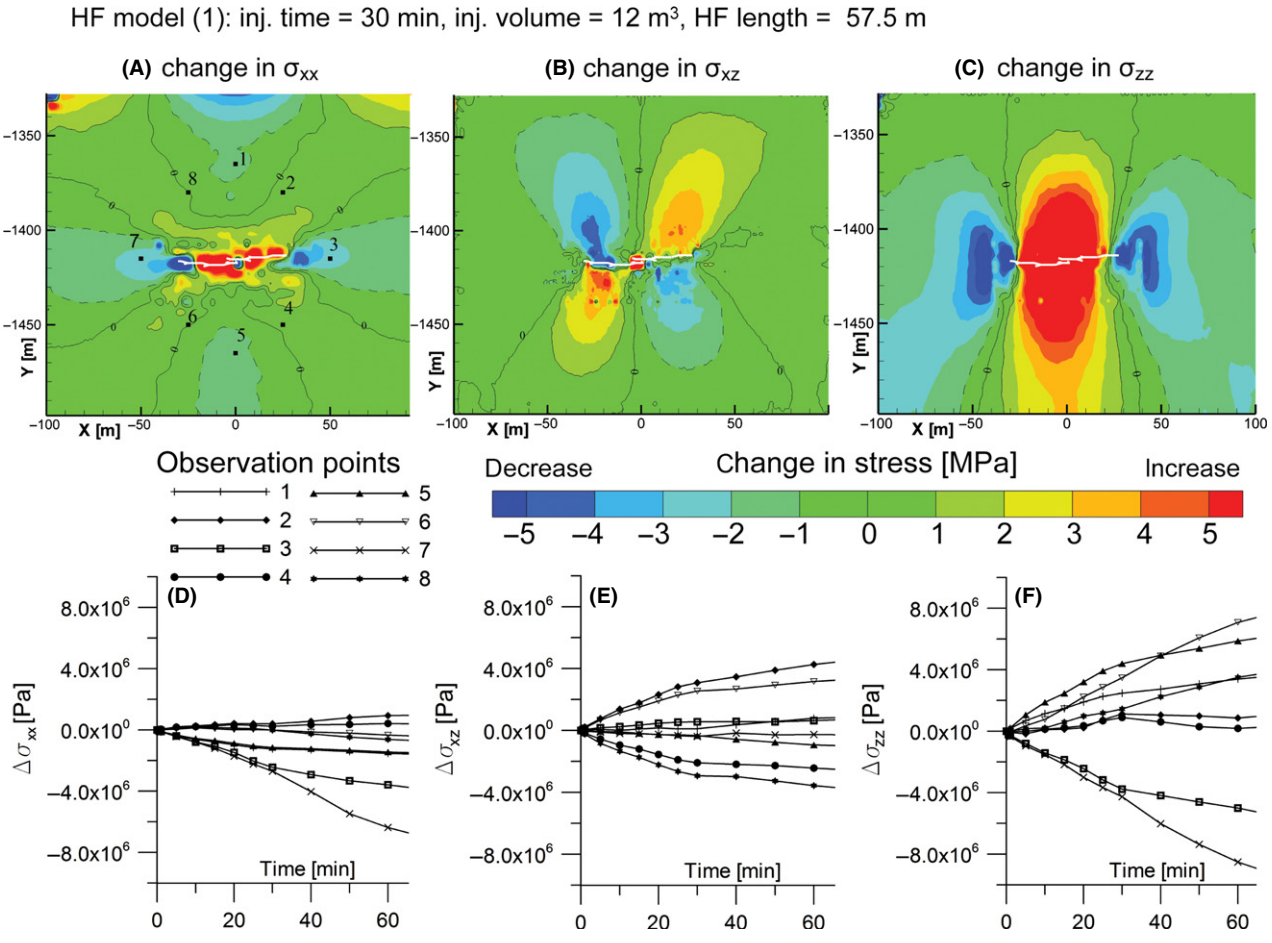

Fig. 7. Hydraulic fracturing model (1): change in (A) horizontal, (B) shear, and (C) vertical stress after 30 min of fluid injection at 400 min^{-1} into a 2-m packed interval. Note that change in stress is computed via a kriging of data obtained from initial stress less stress at a given injection time. (D), (E), and (F) illustrate stress responses during fluid injection for 8 observation points whose location is shown in (A).

DISCUSSION ON THE DEVELOPMENT OF CONNECTED PERMEABILITY

The HF and HS models presented here capture the hydro-mechanical processes accompanying injection of pressurized fluid. Of course, quantitative output derived from these analyses should be treated with caution due to the underlying model simplifications (e.g., 2D versus 3D), and variability and uncertainty associated with the parametric inputs. However, these findings provide considerable insight into the mechanisms, responses, and interactions involved, which can have important implications, in particular for permeability development.

The numerical analyses suggest that the response of a fractured rock mass to fluid injection includes both tensile opening and hydroshear/slip, which are mainly governed by the orientations of the pre-existing natural fracture network and principal stresses, rather than the injection design. However, this finding requires further verification by exploring fluid injection response in other stress-discontinuity configurations. Under the injection metrics and stress-discontinuity discretization used here, tensile opening has been more pronounced than hydroshear. Other configurations, such as the discretization of fracture family 3 through horizontal intact rock bridges and ±15° dipping pre-existing natural fractures, might have resulted in more hydraulic shear. The analysis also illustrated that the stress transfer/shadows accompanying fluid injection are a limiting factor for the development of connected permeability and reservoir enhancement through multiple, adjacent hydraulic fracturing treatments or across an injection interval, because stress transfer serves to confine nearby natural and incipient fractures, limiting their response. This mechanism focuses the development of permeability into a relatively thin layer of rock, instead of across a large volume.

The enhancement of rock permeability due to fluid injection can be illustrated by means of equivalent permeability tensors. The equivalent permeability tensor for the discrete fracture network (DFN) in the refined area of the proposed model is computed as follows: first, average apertures for each fracture family are transformed into parallel permeabilities through the cubic law; next, geometrical properties of the fracture families are combined in space, resulting in a tensor describing the equivalent permeability of the rock mass

$$\mathbf{k} = \sum_{i=1}^{m} \frac{f_i\, a_i^3}{12} \left(\mathbf{I} - \mathbf{n}_i \otimes \mathbf{n}_i\right) \tag{5}$$

where for each fracture family i, until the total number of fractures families m, a is the fracture aperture, f is the frequency of the fracture family i, $\mathbf{I}$ is the identity matrix, $\mathbf{n}$ is the unit vector normal to the fracture family i, and $\otimes$ denotes a tensor product. In matrix form, Eq. 5 leads to

$$\mathbf{k}_{3D} = \begin{bmatrix} k_{xx} & k_{xy} & k_{xz} \\ k_{yx} & k_{yy} & k_{yz} \\ k_{zx} & k_{zy} & k_{zz} \end{bmatrix} \quad ; \quad \mathbf{k}_{2D} = \begin{bmatrix} k_{xx} & k_{xy} \\ k_{yx} & k_{yy} \end{bmatrix} \tag{6}$$

One major advantage of permeability tensors is that their eigenvalues match the magnitude and direction of maximum k_{max} and minimum k_{min} permeability (Király 1969; Berkowitz 2002). Note that permeability is expressed in this work in m^2 and it can be linked to hydraulic/fluid conductivity in m/s via the fluid properties as follows: $K = k\,(\rho_f g / \mu_f)$.

Before fluid injection, the equivalent permeability tensor for the DFN in the refined area of the given model is

$$\mathbf{k} = \begin{bmatrix} 7.5 & 2.0 \\ 2.0 & 1.8 \end{bmatrix} \cdot 10^{-18}\ \mathrm{m}^2$$
$$k_{\max} = 8.1 \cdot 10^{-18}\ ;\ k_{\min} = 1.2 \cdot 10^{-18}\ ;\ \theta = 17 \tag{7}$$

where θ is the counterclockwise angle between the horizontal plane and the direction of k_{max}, in degrees. The initial shape of the permeability tensor reflects that of the initial stress tensor, with k_{max} and k_{min} almost orthogonal to σ_3 and σ_1, respectively.

After injection of 20 m^3 of fluid, the equivalent enhanced permeability tensors for HF model 1 (t = 50 min) and HS model 4 (t = 80 min), are respectively,

HF model 1 :	HS model 4 :
$\mathbf{k} = \begin{bmatrix} 181.9 & 9.2 \\ 9.2 & 2.5 \end{bmatrix} \cdot 10^{-15}\ \mathrm{m}^2$	$\mathbf{k} = \begin{bmatrix} 27.0 & 8.3 \\ 8.3 & 8.5 \end{bmatrix} \cdot 10^{-15}\ \mathrm{m}^2$
$k_{\max} = 182.4 \cdot 10^{-15}$;	$k_{\max} = 30.2 \cdot 10^{-15}$;
$k_{\min} = 2.0 \cdot 10^{-15}$; $\theta = 1$	$k_{\min} = 5.3 \cdot 10^{-15}$; $\theta = 15$

(8)

and gains in permeability in the pressurized rock mass are

HF model 1 :	HS model 4 :
$\mathbf{k}/\mathbf{k}_{\mathrm{init}} = \begin{bmatrix} 24.3 & 4.6 \\ 4.6 & 1.4 \end{bmatrix} \cdot 10^3$	$\mathbf{k}/\mathbf{k}_{\mathrm{init}} = \begin{bmatrix} 3.6 & 4.2 \\ 4.2 & 4.7 \end{bmatrix} \cdot 10^3$
$k_{\max}/\,k_{\max}^{\mathrm{init}} = 22.5 \cdot 10^3$	$k_{\max}/\,k_{\max}^{\mathrm{init}} = 3.7 \cdot 10^3$
$k_{\min}/\,k_{\min}^{\mathrm{init}} = 1.7 \cdot 10^3$	$k_{\min}/\,k_{\min}^{\mathrm{init}} = 4.4 \cdot 10^3$
$\Delta\theta = -16$	$\Delta\theta = -2$

(9)

where $\Delta\theta$ expresses tensor rotation. These data indicate that for both cases, fluid injection is only able to enhance pre-existing magnitudes of the equivalent permeability tensor with limited impact on its direction. This leads to strongly anisotropic preferential flow instead of simple isotropic pressure diffusion, limiting the possibility of volume stimulation. Note that for the hydraulic fracturing case, there is a tensor rotation associated with the increase of anisotropy because of the substantial increase of k_{xx}.

If after fluid injection, the rock mass is suddenly and completely depressurized, gains in permeability reduce to

$$\begin{array}{ll} \text{HF model 1 :} & \text{HS model 4 :} \\ \mathbf{k}/\mathbf{k}_{\text{init}} = \begin{bmatrix} 3.9 & 1.0 \\ 1.0 & 1.0 \end{bmatrix} & \mathbf{k}/\mathbf{k}_{\text{init}} = \begin{bmatrix} 1.2 & 1.0 \\ 1.0 & 1.0 \end{bmatrix} \\ k_{\max}/\,k_{\max}^{\text{init}} = 3.7 & k_{\max}/\,k_{\max}^{\text{init}} = 1.1 \\ k_{\min}/\,k_{\min}^{\text{init}} = 1.4 & k_{\min}/\,k_{\min}^{\text{init}} = 1.0 \\ \Delta\theta = -16 & \Delta\theta = -8 \end{array} \tag{10}$$

These gains in residual rock permeability result from rotation and wedging of neighboring, irregularly shaped rock blocks during fluid injection, which are more pronounced in HF model 1. In these examples, the dilation angle was set to zero; thus, no permanent gains in permeability occur due to fracture dilation during shear, especially for the HS models. Permeability tensors in Eq. 10 clearly illustrate that the gain in permeability is a reversible process without dilation due to the elastic stiffness of the hydraulic fractures. This is in good agreement with some enhanced geothermal systems (EGS) projects where fluid injection led to very small enhancements of permeability, such as in Ogachi, Japan: $k_{stimulated} / k_{initial} \approx 20$ (Kaieda *et al.* 2005). In other EGS projects, for example Basel, Switzerland, and Soultz-sous-Forêt, France, the permanent enhancement of permeability reached factors ranging between 200 and 400 (Evans 2005; Häring *et al.* 2008). These enhancement factors reflect permanent gains in permeability associated with fracture dilation during shear along pre-existing natural fractures. These permeable paths are often comprised of a few major long fractures where the enhancement of permeability is focused (Evans 2005). This leads also to increased anisotropic preferential flow, instead of developing permeability uniformly across a large rock volume. Similar effects can be inferred from the seismic cloud obtained for the Cooper Basin project, Australia (Bendall *et al.* 2014).

The EGS examples cited here also suggest that the reactivation of long-persistent fractures via hydraulic shearing is likely to produce significant induced seismicity. Permeability tensors in Eq. 10 also suggest that proppant injection is critical for achieving permanent apertures.

The numerical analyses performed, together with the points discussed above, suggest that in tight rock masses, it will be difficult to develop connected permeability across a large volume through a single hydraulic fracturing (HF) or hydraulic shearing (HS) injection. This may be solved by first inducing a stack of hydraulic fractures, as is commonly done during multistage hydraulic fracturing (Dusseault & McLennan 2011), and then performing a HS injection. Doing so will permit pressure diffusion across a larger volume of rock during the second-stage injection, with possible reactivation in shear of favorably oriented connected natural fractures. Aside from logistical constraints, such a strategy merits verification through the *in situ* experiment planned. Moreover, in the first stage of injection, the development of a stack of tensile hydraulic fractures can be optimized by utilizing small-packed intervals where the borehole intersects natural fractures orthogonal to σ_3 (identified in borehole televiewer logs). Again, this type of control is not possible via a single fluid injection in an open borehole, where the rock mass response to injection will mostly depend on the geometrical and hydraulic properties of the natural pre-existing fracture network. Although these findings are specific to massive crystalline rocks, which are primarily encountered in deep mining and EGS projects, they also merit consideration in future research related to the improvement of reservoir permeability in tight sedimentary rocks, especially where fluid flow in fractures significantly exceeds flow into the rock matrix. Despite simulated injection times on the order of 60 minutes, the highlighted processes are also likely to develop during longer fluid injections of hours, days, or weeks, as is common in EGS practices. For example, the orientation and direction of development of anisotropic permeability highlighted in the first stages of a hydraulic treatment is expected to persist during a longer injection. A change in the direction of enhancement may occur if the propagating front encounters and pressurizes a zone of high pre-existing natural permeability. This mechanism explains the deviation of a seismic cloud associated with an injection of pressurized fluid, as experienced at Basel (Häring *et al.* 2008). Based on the results presented in this paper, a conceptual model is presented in Fig. 8 illustrating important interactions and responses related to the enhancement of reservoir permeability, especially for a multistage framework. Key considerations to be further investigated through the *in situ* experiment and continued numerical modeling are as follows:

(1) Investigate the capacity of a rock mass to attenuate stress transfer in order to propose a critical distance between the stack of hydraulic fractures.
(2) Consider different initial permeability and stress states, that is, extensional and strike-slip regimes, as well as highly connected fracture networks with different geometries.
(3) Consider the ability to generate permanent apertures with and without proppant injection. This includes the role of asperities and dilation in the elastic or inelastic behavior of fractures.
(4) Assess the possibility of hydroshearing and associated fracture dilation between the stack of hydraulic fractures, as well as their ability to increase connectivity and allow fluid flow at full-size reservoir scale.
(5) Confirm model results showing that rock mass deformations in the form of uplift and tilt are low for a single hydraulic fracturing or hydraulic shearing treatment and that displacement is attenuated by the deformation

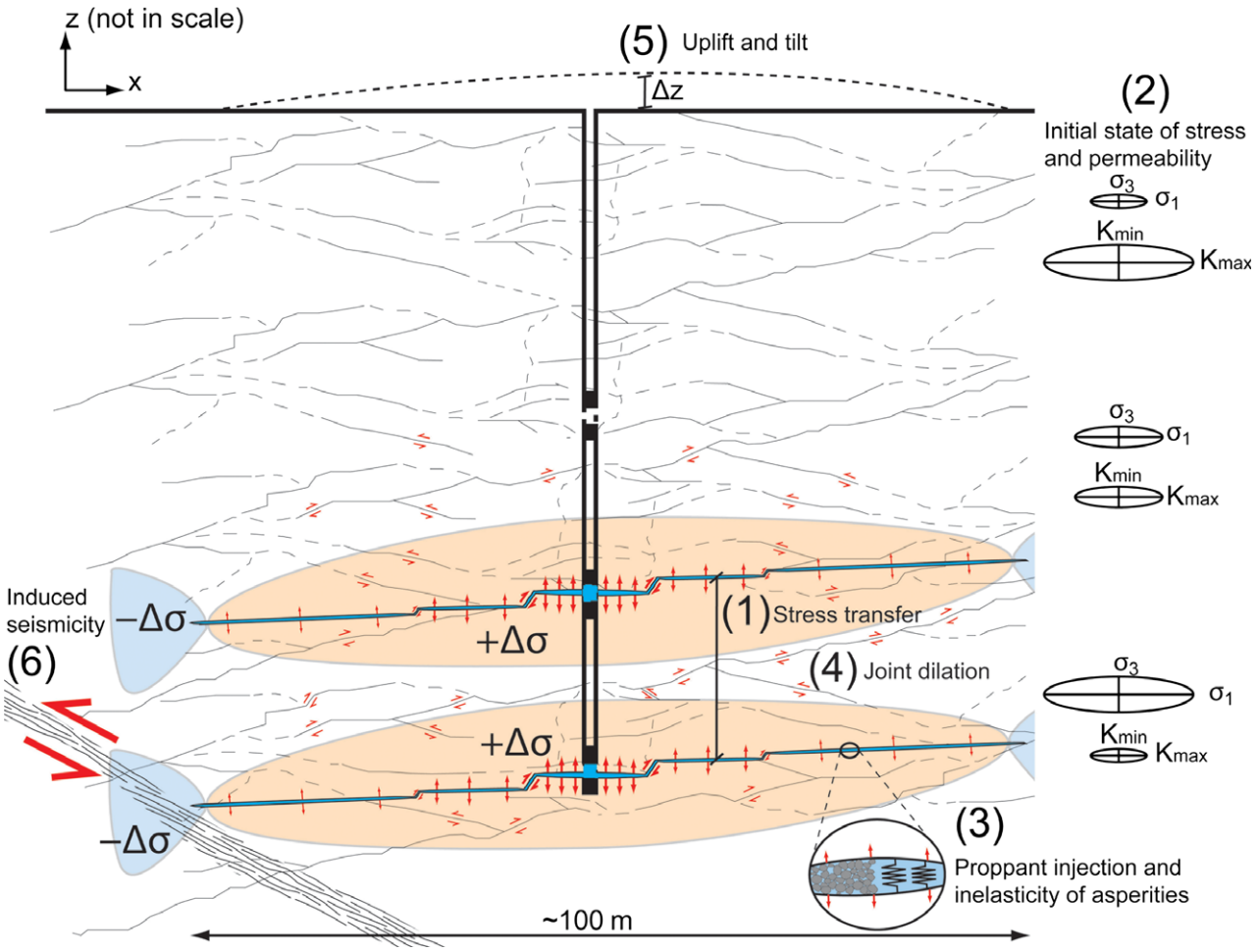

Fig. 8. Schematic cross-section illustrating issues related to development of connected permeability by injection of pressurized fluid: (1) stress transfer between principal hydraulic fractures and its attenuation by intact rock blocks; (2) *in situ* stress state and initial permeability; (3) permanent aperture of tensile hydraulic fractures due to inelasticity of asperities or because of proppant injection; (4) permeability enhancement associated with fracture dilation under shearing; (5) generation of uplift and tilt, as well as (6) induced seismicity.

of the adjacent rock blocks. Massive enhancement can generate nonnegligible uplifts and tilts and therefore needs to be further investigated.

(6) Assess the georisk related to induced seismicity, such as the pressurization of critically stressed faults during and after preconditioning, leading to fault slip and seismicity.

Finally, as regards to long-term exploitation of an enhanced geothermal system, it is also critical to consider the time-dependent deterioration of reservoir permeability due to fracture closure associated with fluid pressure leak off and dissipation, clogging of fracture apertures due to mineral precipitations, and other impacts on permeability associated with thermal depletion and compaction of the reservoir. These issues need to be approached through implementation of more advanced thermal–hydraulic–mechanical–chemical (THMC) modeling, which can account for long-term performance over year to decade timescales. Simulation of all these processes during long periods of fluid flow may be achieved by selecting only the dominant, governing mechanisms (Miller 2015; Rutqvist 2015; Weis 2015). Based on these models, a long-term exploitation design should minimize these problems and enable maximum resource extraction.

CONCLUSIONS

Stress transfer associated with fluid injection is a key limiting factor for developing interconnected rock mass permeability and reservoir enhancement at depth, in particular for a network of natural, nonpersistent fractures. Tensile opening of a hydraulic fracture will generate an increase in stress which limits the response of neighboring fractures in both tensile opening and hydraulic shearing. The result is that hydraulic stimulation across a wide interval will be prone to produce a thin layer of enhanced permeability

instead of a large volume. This will lead to strongly anisotropic flow. Moreover, there are limited options via the injection design to influence the rock mass response, for instance by promoting hydraulic shearing over tensile opening, especially when long, optimally oriented natural fractures are sparse. Instead, the system response will mainly depend on the geometrical characteristics of the preexisting natural fracture network and orientation of the *in situ* stress field. These findings suggest that deep reservoir enhancement for geofluids extraction and circulation can be better approached by targeting fluid injections in small-packed intervals.

However, additional work is required to assess the effectiveness of permeability enhancement in deep, fractured rock masses where the *in situ* stress state, fracture network geometry, and initial connectivity differ. Further testing is also required to investigate stress transfer between hydraulic fractures in the case of a multistage design, as well as the potential for shearing between the stack of tensile hydraulic fractures. Verification and validation of these results will be explored through the *in situ* experiments for which this modeling was performed. Other related issues that will be explored include stress field modification for managing high stresses during deep mining and the minimization of induced seismicity accompanying fluid injection for geothermal and shale gas production. These issues underscore the challenges faced in the design of deep reservoir enhancement and its exploitation, and the need for continued research.

ACKNOWLEDGEMENTS

This work was carried out within the framework of the CEMI Newcrest mine-back experiment and was sponsored in part by the Swiss National Science Foundation (Project No. 146075) and Natural Sciences and Engineering Research Council of Canada. The authors wish to thank Newcrest for provision of the rock mass property data and permission to publish, in particular Dr. Geoff Capes. We also gratefully thank Dr. Steve Ingebritsen and Dr. Tom Gleeson for this special issue on crustal permeability and for their comments which significantly improved this paper. Constructive comments and time allocated to this work of two anonymous reviewers were also much appreciated by the authors.

REFERENCES

Anderson EM (1951) *The Dynamics of Faulting*. Oliver & Boyd, Edinburgh. 206 pp.

Araneda OA, Morales RF, Rojas EG, Henríquez JO, Molina RE (2007) Rock preconditioning application in virgin caving condition in a panel caving mine, CODELCO Chile El Teniente Division. In: *Proceedings International Symposium, Deep and High Stress Mining*, pp. 111–20. Australian Centre for Geomechanics, Perth, Australia.

Bendall B, Hogarth R, Holl H, McMahon A, Larking A, Reid P (2014) Australian Experiences in EGS Permeability Enhancement – A Review of 3 Case Studies. In: Thirty-Ninth Workshop on Geothermal Reservoir Engineering, Stanford University, California.

Berkowitz B (2002) Characterizing flow and transport in fractured geological media: a review. *Advances in Water Resources*, **25**, 861–84.

Bunger AP, Jeffrey RG, Kear JP, Zhang XP, Morgan M (2011) Experimental investigation of the interaction among closely spaced hydraulic fractures. In: 45th US Rock Mechanics / Geomechanics Symposium, June 26–29, 2011, San Francisco, California.

Cappa F (2006) Role of fluids in the hydromechanical behavior of heterogeneous fractured rocks: *in situ* characterization and numerical modelling. *Bulletin of Engineering Geology and the Environment*, **65**, 321–37.

Durham WB (1997) Laboratory observations of the hydraulic behavior of a permeable fracture from 3800 m depth in the KTB pilot hole. *Journal of Geophysical Research*, **102**, 18405–16.

Dusseault M, McLennan J (2011) Massive multistage hydraulic fracturing: Where are we? In: 45th US Rock Mechanics/ Geomechanics Symposium, San Francisco, 14 pp.

Eaton D, van der Baan M, Birkelo B, Tary J-B (2014) Scaling relations and spectral characteristics of tensile microseisms: evidence for opening/closing cracks during hydraulic fracturing. *Geophysical Journal International*, **196**, 1844–57.

Evans K (2005) Permeability creation and damage due to massive fluid injections into granite at 3.5 km at Soultz: 2. critical stress and fracture strength. *Journal of Geophysical Research*, **110**, 14.

Evans KF, Genter A, Sausse J (2005) Permeability creation and damage due to massive fluid injections into granite at 3.5 km at Soultz: 1. borehole observation. *Journal of Geophysical Research*, **110**, 1–19.

Fairhurst C (2013) Fractures and fracturing: hydraulic fracturing in jointed rock. In: *Effective and Sustainable Hydraulic Fracturing* (eds Bunger A, McLennan J, Jeffrey R), pp. 47–79. InTech, Rijeka, Croatia.

Häring M, Schanz U, Ladner F, Dyer B (2008) Characterisation of the Basel 1 enhanced geothermal system. *Geothermics*, **37**, 469–95.

Hsiung S, Chowdhury A, Nataraja M (2005) Numerical simulation of thermal-mechanical processes observed at the Drift-Scale Heater Test at Yucca Mountain, Nevada, USA. *International Journal of Rock Mechanics and Mining Sciences*, **42**, 652–66.

Ingebritsen S, Manning C (2010) Permeability of the continental crust: dynamic variations inferred from seismicity and metamorphism. *Geofluids*, **10**, 193–205.

Itasca (2013) UDEC 5.0 Universal Distinct Element Code, Itasca Consulting Group Inc, Minneapolis, USA.

Jeffrey RG, Bunger A, Lecampion B, Zhang X, Chen ZR, van As A, Allison DP, de Beer W, Dudley JW, Siebrits E, Thiercelin M, Mainguy M (2009) Measuring Hydraulic Fracture Growth in Naturally Fractured Rock, SPE Annual Technical Conference and Exhibition, 4-7 October, New Orleans, Louisiana, http://dx.doi.org/10.2118/124919-MS.

Jung R (2013) EGS – Goodbye or Back to the Future. In: *Effective and Sustainable Hydraulic Fracturing* (eds Bunger A, McLennan J, Jeffrey R), pp. 95–121. InTech, Rijeka, Croatia.

Kaieda H, Jones R, Moriya H, Sasaki S, Ushijima K (2005) Ogachi HDR reservoir evaluation by AE and geophysical methods, In: Proceedings of World Geothermal Congress.

Kaiser P, Valley B, Dusseault M, Duff D (2013) Hydraulic fracturing mine back trials – design rationale and project status.

In: *Effective and Sustainable Hydraulic Fracturing* (eds Bunger A, McLennan J, Jeffrey R), pp. 877–91. InTech, Rijeka, Croatia.
Király L (1969) Anisotropy and heterogeneity within jointed limestone. *Eclogae Geologicae Helvetiae*, **62**, 613–9.
Louis C (1969) A study of groundwater flow in jointed rock and its influence on the stability of rock masses. Technical Report 9, Rock Mechanics, Imperial College, London, United Kingdom.
Luthi S, Souhaité P (1990) Fracture apertures from electrical borehole scans. *Geophysics*, **55**, 821–33.
Miller S (2015) Modeling enhanced geothermal systems and the essential nature of large-scale changes in permeability at the onset of slip. *Geofluids*, **15**, 338–49.
Pine RJ, Batchelor AS (1984) Downward migration of shearing in jointed rock during hydraulic injections. *International Journal of Rock Mechanics and Mining Sciences*, **21**, 249–63.
Polski Y, Capuano L, Finger J, Huh M, Knudsen S, Chip Mansure A, Raymond D, Swanson R (2008) Enhanced Geothermal Systems (EGS) Well Construction Technology Evaluation Report. Department of Energy, USA, Tech Rep, U.S.
Preisig G, Cornaton FJ, Perrochet P (2012) Regional flow simulation in fractured aquifers using stress-dependent parameters. *Groundwater*, **50**, 376–85.
Rutqvist J (2015) Fractured rock stress-permeability relationships from *in situ* data and effects of temperature and chemical-mechanical couplings. *Geofluids*, **15**, 48–66.
Rutqvist J, Stephansson O (1996) A cyclic hydraulic jacking test to determine the *in situ* stress normal to a fracture. *International Journal of Rock Mechanics and Mining Sciences Geomechanics Abstracts*, **33**, 695–711.
Snow D (1970) The frequency and apertures of fractures in rock. *International Journal of Rock Mechanics and Mining Sciences*, **7**, 23–40.
Tsang Y, Witherspoon P (1981) Hydromechanical behaviour of a deformable rock fracture subject to normal stress. *Journal of Geophysical Research*, **86**, 9287–98.
Vincent M (2013) Five things you didn't want to know about hydraulic fractures. In: *Effective and Sustainable Hydraulic Fracturing* (eds Bunger A, McLennan J, Jeffrey R), pp. 81–93. InTech, Rijeka, Croatia.
Weis P (2014) The dynamic interplay between saline fluid flow and rock permeability in magmatic-hydrothermal systems. *Geofluids*, **15**, 350–71.
Whiterspoon P, Wang J, Iwai K, Gale J (1980) Validity of cubic law for fluid-flow in a deformable rock fracture. *Water Resources Research*, **16**, 1016–24.
Zangeneh N, Eberhardt E, Bustin R (2012) Application of the distinct-element method to investigate the influence of natural fractures and *in situ* stresses on hydrofrac propagation. In: 46th US Rock Mechanics/Geomechanics Symposium, Chicago, 8 pp.

GEOFLUIDS

Volume 15, Number 1 and 2, February 2015

ISSN 1468-8115

CONTENTS